Materials Research Bulletin 165 (2023) 112322

Contents lists available at ScienceDirect

Materials Research Bulletin

journal homepage: www.elsevier.com/locate/matresbu

Short communication

Decrypting the growth of anodic TiO_2 nanotube layers in eco-friendly fluoride-free nitrate-based electrolyte for enhanced photocatalytic degradation of organic pollutants

Guru Karthikeyan Thirunavukkarasu [a,b,*], Muhammad Bilal Hanif [a], Viktoriia Liapun [a,c], Karol Hensel [d], Jaroslav Kupčík [b,e], Jan Lorincik [f], Ivan Elantyev [f], Olivier Monfort [a], Martin Motola [a,*]

[a] Department of Inorganic Chemistry, Faculty of Natural Sciences, Comenius University Bratislava, Ilkovicova 6, 842 15 Bratislava, Slovakia
[b] Institute of Inorganic Chemistry of the Czech Academy of Sciences, Husinec-Řez 250 68, Czech Republic
[c] Department of Environmental Ecology and Landscape Management, Faculty of Natural Sciences, Comenius University Bratislava, Ilkovicova 6, 842 15 Bratislava, Slovakia
[d] Division of Environmental Physics, Faculty of Mathematics, Physics and Informatics, Comenius University Bratislava, Mlynska Dolina, 842 48 Bratislava, Slovakia
[e] Institute of Physics of the Czech Academy of Sciences, Na Slovance 1999/2, 182 00 Prague 8, Czech Republic
[f] Research Centre Řez, Hlavni 130, Husinec-Řez 250 68, Czech Republic

ARTICLE INFO

Keywords:
Anodization
TiO_2 nanotube layers
Photocatalysis
Fluoride-free electrolyte
Nitrate-based electrolyte
Methylene blue degradation

ABSTRACT

Anodic TiO_2 nanotube (TNT) layers were prepared in eco-friendly fluoride-free organic-aqueous-based electrolytes containing cerium ammonium nitrate. Nanotubes with controllable morphology (tube diameter and tube length) and surface features (porosity and surface roughness) were obtained by varying percentual ratios of ethylene glycol ($E_{x\%}$) and water ($W_{y\%}$) in the electrolyte ($E_{x\%}W_{y\%}$). Obtained TNT layers were studied for photocatalytic degradation of methylene blue (MB) under UVA irradiation. The most promising, TNT layers were prepared in $E_{75\%}W_{25\%}$ electrolyte with a thickness of approx. 1.9 μm with a tube diameter of approx. 33 nm, and exhibited the highest photocatalytic degradation rate (k = 0.0151 min^{-1}).

1. Introduction

Since the growth of nanoporous/nanotubular layered structures via electrochemical anodization of Ti in fluoride-based electrolytes, as reported by Assefpour-Dezfuly et al. [1], TiO_2 nanotube (TNT) layers have become one of the most promising nanostructures over the past decades. Indeed, TNT layers are attractive due to their 1D structure, which provides unique properties, e.g., quantum confinement effects, improved e^-/h^+ separation, and transport [2], thus being a promising photocatalyst [3,4]. Photocatalysis is attractive because it can potentially utilize sunlight to produce reactive oxygen species (ROS) that could substantially eliminate and convert pollutants into harmless substances [5–10]. In the context of water treatment, photocatalysis has gained significant importance as a promising method for the removal of pollutants from water [11,12].

TNT layers prepared via electrochemical anodization provide controllable nanotubular morphology (i.e., tube diameter, layer thickness, and wall thickness) [13,14]. Indeed, the morphology is directly controlled by e.g., the anodization time, applied potential, current density, and electrolyte type [2,15]. Nowadays, TNT layers are prepared in the popular aqueous-organic-based (ethylene glycol, diethylene glycol, glycerol, etc.) electrolytes containing fluoride ions (as well as using other halogens e.g., chlorides, bromides) [13,14,16–18]. Indeed, fluoride ions were considered irreplaceable for nanotubular formation via the field-assisted dissolution of the formed TiO_2 layer [2,13,14,19]. However, fluoride ions (including other halogens) are deemed hazardous to the environment [20–22]. Moreover, the use of halogens in the electrolytes causes adhesion issues between the Ti metal and TNT layer, that is, it leads to the TNT layer being easily peeled off from the underlying Ti metal [23,24]. Recently, fluoride-free (halogen-free) alternatives using nitrates-based electrolytes such as $AgNO_3$, $Sr(NO_3)_2$, KNO_3, $NaNO_3$, and NH_4NO_3 were reported [23,25–27]. TNT layers

* Corresponding authors at: Department of Inorganic Chemistry, Faculty of Natural Sciences, Comenius University Bratislava, Ilkovicova 6, 842 15 Bratislava, Slovakia.
E-mail addresses: thirunavukkarasu1@uniba.sk (G.K. Thirunavukkarasu), martin.motola@uniba.sk (M. Motola).

https://doi.org/10.1016/j.materresbull.2023.112322
Received 19 January 2023; Received in revised form 7 April 2023; Accepted 2 May 2023
Available online 3 May 2023

formed in nitrate-based electrolytes do not follow the field-assisted dissolution theory but instead follow the oxygen bubble mold effect, viscous flow model, and electronic current theory [28–31]. For example, Lu et al. [25]. showed that TNT layers are formed through the oxygen bubble mold effect in fluoride-free nitrate-based electrolytes, that is, electronic current leads to oxygen evolution, which in turn creates pores. However, there is still debate within the scientific community regarding the mechanism of TNT layer growth in nitrate-based electrolytes. As an advantage, TNT layers are prone to grow to a few micrometers within a short anodization time in nitrate-based electrolytes, with only a handful of reports published to date [23,25–27]. Additionally, TNT layers synthesized in Ag, Sr, K, and Na-nitrates led to the decoration of these elements on the nanotubes, thereby reducing the optical bandgap (E_g) and promoting e^-/h^+ separation [23]. Such decorated fluoride-free TNT layers synthesis using electrolytes containing rare earth elements has not yet been explored. Among the rare earth elements, Ce is attractive because of its interconvertible oxidation states (Ce^{3+}/Ce^{4+}), reduces the E_g of TiO_2, prevent e^-/h^+ recombination, and could generate H_2O_2 *in-situ*, thereby increasing the efficiency of photocatalytic process [6,32,33].

Optimizing the TNT layers morphology by varying the electrolyte content in fluoride-based electrolytes [19,34,35] and the influence on nanotubes morphology in photocatalytic performance [36–41] have already been reported. However, optimization of the TNT layer morphology by varying the electrolyte content in fluoride-free nitrate-based electrolytes has not yet been reported. Here, we prepared the TNT layers with different morphology and surface properties via electrochemical anodization technique in 0.5 wt% cerium ammonium nitrate (CAN, $(NH_4)_2[Ce(NO_3)_6]$) electrolyte with varying the percentual ratios of ethylene glycol (E) and water (W) content. Finally, the overall influence of different TNT layers features on the photocatalytic degradation of methylene blue (MB) under UVA irradiation was investigated. In addition, the production of $HO^{\cdot}$ radicals under UVA irradiation (essential for the photocatalytic process) was observed using coumarin as a fluorescence probe and was analyzed using a fluorescence spectrophotometer.

2. Materials and methods

2.1. Fluoride-free TNT layer synthesis

Ti foil (1 × 3 cm, Sigma Aldrich, Slovakia, 0.127 mm thick, 99.7% purity) was used as a substrate for the synthesis of fluoride-free TNT layers. Prior to anodization, Ti foil was cleaned by sonication in isopropyl alcohol (IPA, Central Chem, Slovakia) for 2 min and subsequently dried using an air blower. Electrochemical anodization was carried out in a DC power supply (ET systems GmbH, Germany) at a maximum current of 0.2 A (i.e., current would not exceed beyond 0.2 A) and an anodization time of 5 min. Anodization potential was varied to maintain a constant current flow during the TNT layer synthesis. Ti foil was used as a working electrode, and a graphite rod (3 cm^2, Chenjianqing, China) was used as a counter electrode. The electrodes are kept at a mutual distance of 1.5 cm. The electrolyte was composed of 0.5 wt% of cerium ammonium nitrate dissolved in 200 mL of different vol% compositions of ethylene glycol (E) and distilled (DI) water (W). The different electrolyte compositions were the following: $E_{100\%}W_{0\%}$ (100% ethylene glycol and 0% DI water), $E_{75\%}W_{25\%}$ (75% ethylene glycol and 25% DI water), $E_{50\%}W_{50\%}$ (50% ethylene glycol and 50% DI water), $E_{25\%}W_{75\%}$ (25% ethylene glycol and 75% DI water), and $E_{0\%}W_{100\%}$ (0% ethylene glycol and 100% DI water). After anodization, the prepared TNT layers were sonicated in IPA for 15 s and subsequently dried using an air blower to remove the electrolytes leftovers. Finally, the as-prepared TNT layers were annealed in air at 450 °C for 2 h at a rate of 2 °C/min to form anatase TiO_2. Further, detailed information about the characterization techniques and photocatalytic degradation process for the prepared TNT layers are given in ESI.

3. Results and discussion

The morphological features of the obtained TNT layers were observed through field emission scanning electron microscopy (FESEM, Figs. 1(a–e) and S1) and transmission electron microscope (TEM, Figs. 1f and S2). It was evidently revealed that there is a clear difference in nanotubular morphology, including tube diameter and layer thickness. Indeed, the morphology significantly varied due to the use of different electrolyte compositions. For instance, no nanotubular morphology was observed for TNT layers prepared in $E_{100\%}W_{0\%}$. Indeed, the Ti foil was etched, thus forming nanopits in a few places (Fig. 1a). Due to the viscosity of the ethylene glycol, the bubble mold effect and electronic current theory are possibly suppressed, preventing the pore formation on Ti foil. The viscosity of the ethylene glycol affects the growth of the nanotubes, smoothness, and slow down the crystal growth [42]. Moreover, when applying a high potential (100 V), a current reached approx. 0.14 A (Fig. S3) (i.e., 0.2 A cannot be maintained as mentioned in the experimental part). Nevertheless, in case water was added to the electrolyte, the current density reached the value of 0.2 A (Fig. S3) and the formation of nanotubular morphology was observed (Fig. 1(b–f)).

As expected, TNT layers with different morphological features were obtained by varying the ratio between E:W (Fig. 2(a,b)). Indeed, 1.9 μm thick TNT layers with approx. 33 nm were obtained using $E_{75\%}W_{25\%}$. In contrast, nanotubes with decreased tube diameter were obtained after increasing the water content ($E_{50\%}W_{50\%}$, $E_{25\%}W_{75\%}$, and $E_{0\%}W_{100\%}$). Despite decrease in tube diameter (to approx. 25 nm), TNT layers with thickness of approx. 2.5 μm were obtained in $E_{0\%}W_{100\%}$. These results indicate an evident influence of the E:W ratio in obtaining different nanotubular morphologies. Further, clear bundles of few nanotubes could be observed through TEM (Figs. 1f and S2). Since, the preparation of samples for TEM is destructive for the TNT layers, i.e., TNT layers were scrapped from the underlying Ti substrate. Therefore, calculation of morphological features through TEM may not be representative, hence images observed through FESEM were used for calculating tube diameter, wall thickness, and tube length for the TNT layers. There are multiple reports on the impact of water content in obtaining nanotubular morphology in fluoride-based electrolytes [35,43,44]. Here, we report, for the first time, the influence of water content on nanotubular morphology in fluoride-free nitrate-based electrolytes. Indeed, the morphological features are essential for the efficient application of any material in e.g., photocatalysis [41].

Additionally, the TNT layers porosity (*P*) and surface roughness factor (*rf*) were estimated according to the following equations [45,46].

$$P = 1 - \frac{2\pi w(w + D)}{\sqrt{3}(D + 2w)^2} \quad (1)$$

$$rf = \frac{2(1 - P)}{w} \quad (2)$$

where *w* is the wall thickness and *D* is the tube diameter of the nanotube. The highest porosity (approx. 36%) was calculated for TNT layers prepared in $E_{75\%}W_{25\%}$, which also exhibited the highest surface roughness factor (approx. 90 μm^{-1}) (Fig. 2c). TNT layers prepared in other electrolytes i.e., $E_{50\%}W_{50\%}$, $E_{25\%}W_{75\%}$, and $E_{0\%}W_{100\%}$ possess a similar mean ratio between D and w of approx. 0.5, thereby similar calculated porosity (approx. 20%) was observed. Quitério et.al. [47] reported the porosity of approx. 5.6% for TNT layers prepared in fluoride-containing electrolyte with different diameters and wall thickness. Interestingly, yet having similar porosity, these TNT layers possessed different surface roughness factors of 60, 71, and 64 μm^{-1}, respectively. It is worth noting that higher porosity and surface roughness is related to an increase in the specific surface area, thereby improving the overall application potential in photocatalytic process [48–51].

Further, structural characterization using x-ray diffractometer in grazing incidence mode (GI-XRD) revealed the crystalline phases of the

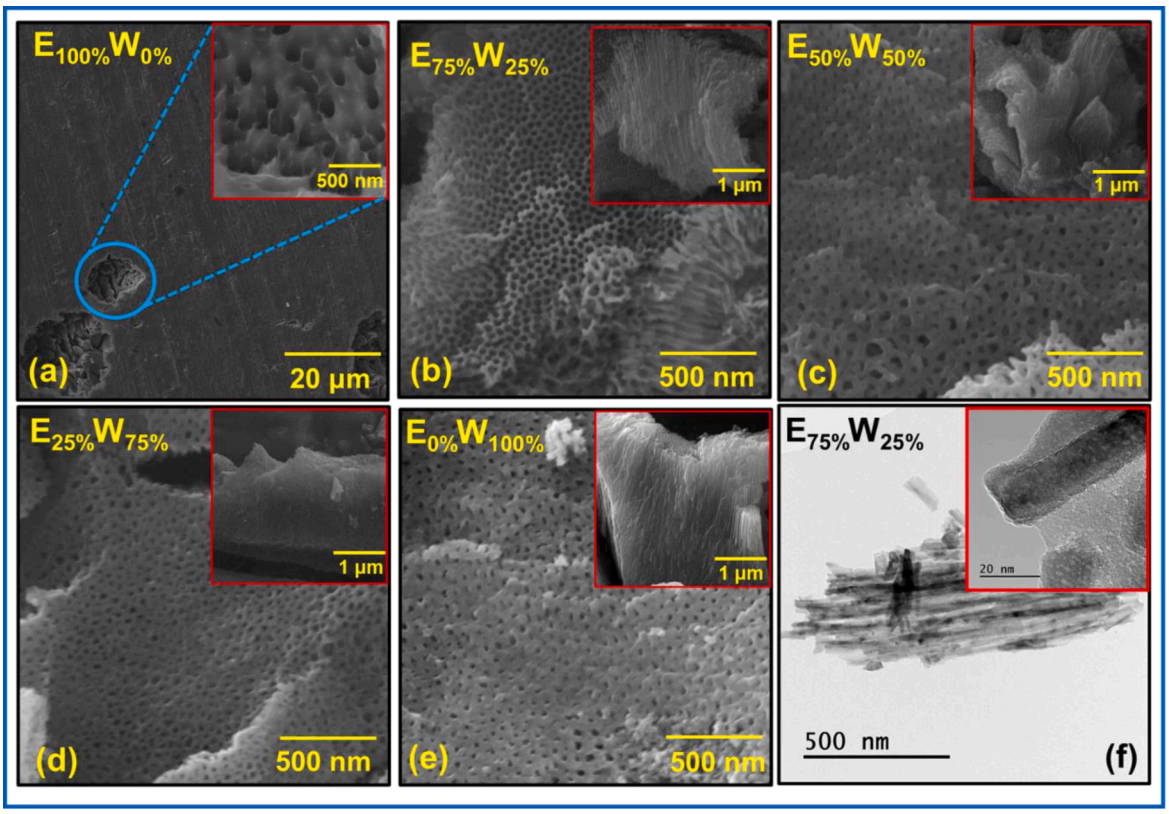

Fig. 1. Representative FESEM images showing both top views and cross-sectional views (inset) of the TNT layers prepared in cerium ammonium nitrate electrolyte with different compositions of ethylene glycol and water: (a) $E_{100\%}W_{0\%}$, (b) $E_{75\%}W_{25\%}$, (c) $E_{50\%}W_{50\%}$, (d) $E_{25\%}W_{75\%}$, and (e) $E_{0\%}W_{100\%}$. (f) Representative TEM images of the optimized sample $E_{75\%}W_{25\%}$ and inset shows the high-resolution image of individual nanotube.

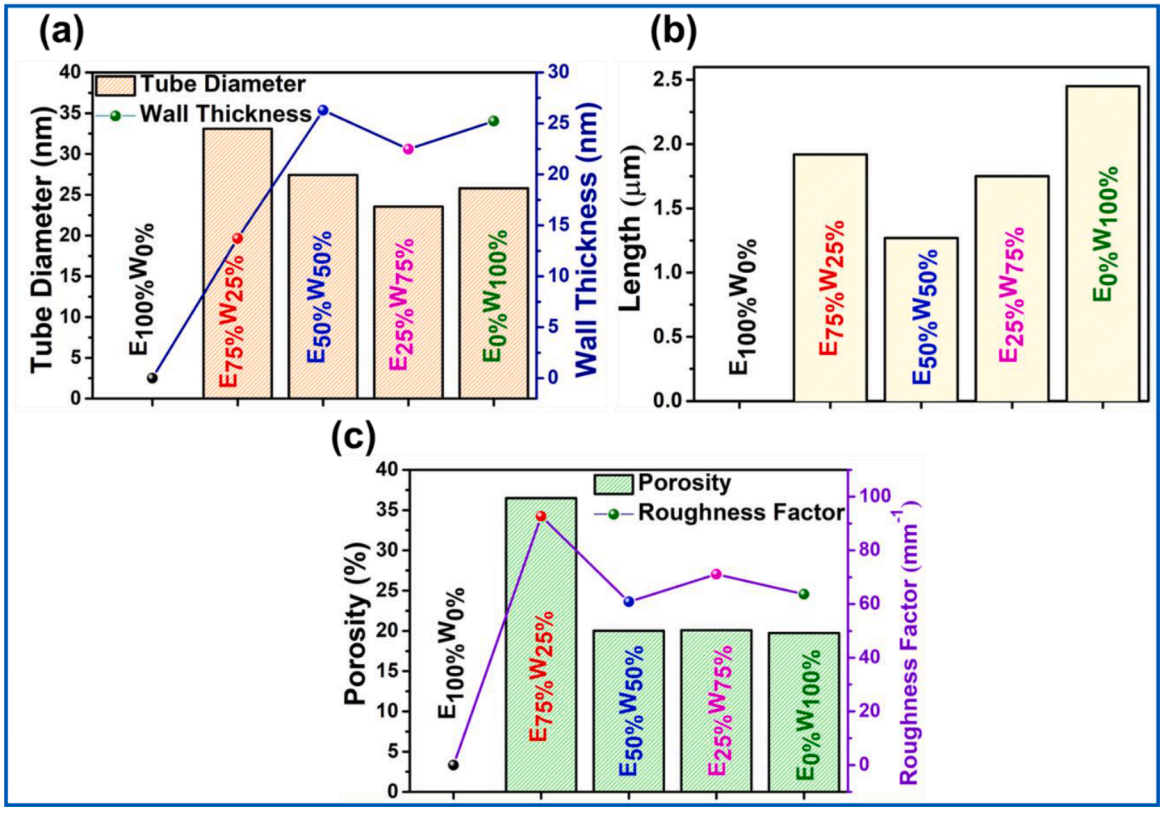

Fig. 2. Tube diameter, wall thickness, tube length, porosity, and surface roughness factor calculated from the FESEM images of the prepared TNT layers are depicted in (a), (b), and (c), respectively.

TNT layers prepared in different electrolyte compositions (Fig. 3a). TNT layers prepared in $E_{100\%}W_{0\%}$ showed a major presence of hexagonal Ti diffraction peaks ($P6_3/mmc$; ICCD 00–044–1294) along with a minor anatase phase TiO_2 diffractions. These results also correlate with the FESEM images (Fig. 1a), which revealed the etching of Ti foil without the formation of the nanotubular structure. Nevertheless, all TNT layers prepared in electrolytes containing water (i.e., $E_{75\%}W_{25\%}$, $E_{50\%}W_{50\%}$, $E_{25\%}W_{75\%}$, and $E_{0\%}W_{100\%}$) exhibited crystalline anatase TiO_2 phase ($P4_2/mnm$; ICCD 01–086–1157) along with hexagonal Ti diffraction peaks (originating from the underlying Ti foil). TNT layers obtained

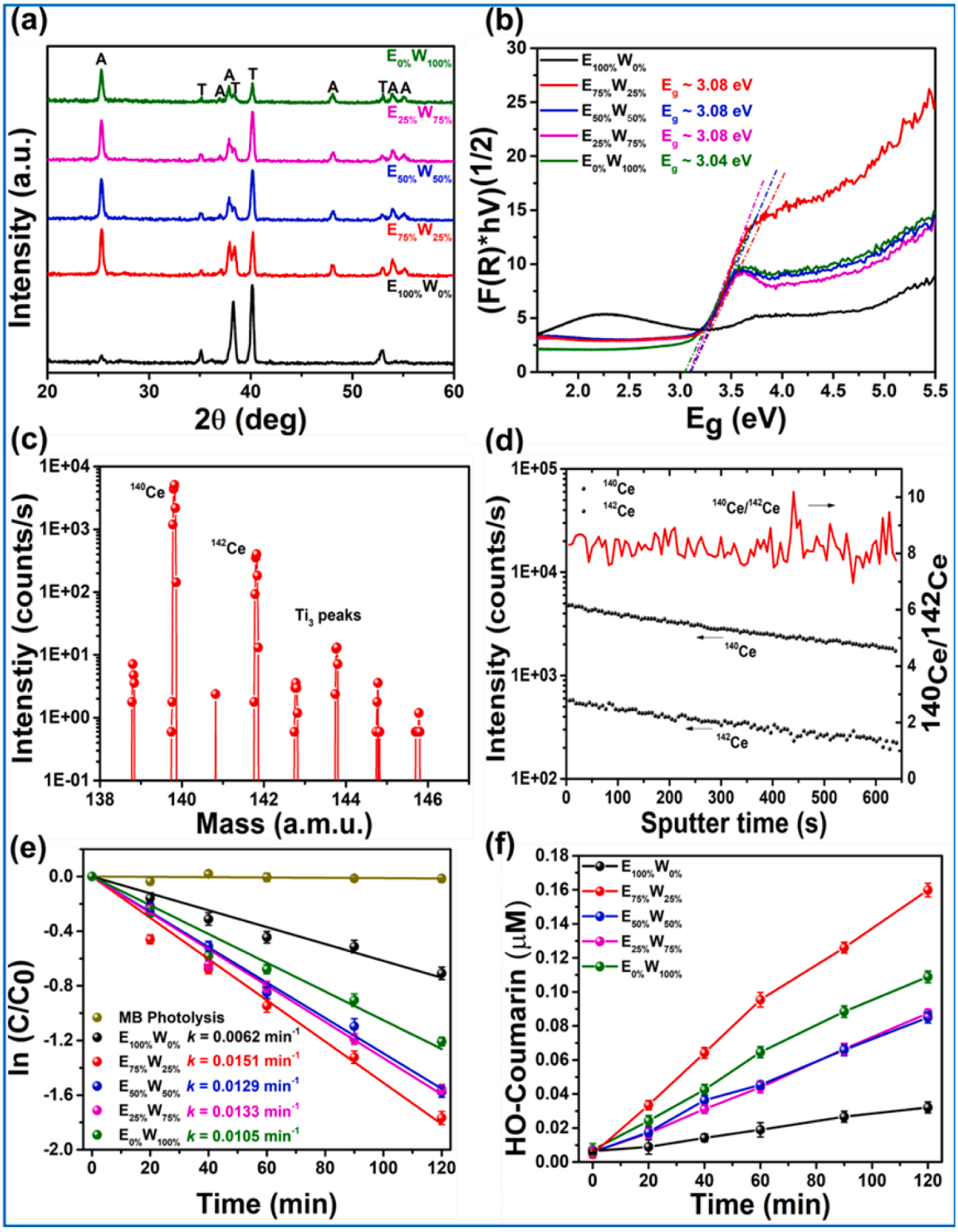

Fig. 3. Structural, optical, elemental composition, and photocatalytic characterization of the prepared TNT layers in $E_{100\%}W_{0\%}$, $E_{75\%}W_{25\%}$, $E_{50\%}W_{50\%}$, $E_{25\%}W_{75\%}$, and $E_{0\%}W_{100\%}$ electrolytes. (a) XRD pattern, (b) Tauc's plot depicting the E_g calculated from the UV–Visible diffuse reflectance spectra, (c) SIMS mass spectrum at 138 a.m.u. – 146 a.m.u. of the representative sample $E_{75\%}W_{25\%}$, (d) SIMS depth profiling of Ce, (e) The linearized pseudo-first-order plots of $\ln(C/C_0)$ versus time for photocatalytic degradation of MB, and (f) production of $HO^{\cdot}$ radicals using coumarin as a fluorescent probe.

from fluoride-free nitrate-based electrolytes exhibit morphological and structural features comparable to those of TNT layers prepared in fluoride-based electrolytes (Table S1) [17,23,25,52,53]. However, the time taken to grow TNT layers of up to 2.5 μm using a fluoride-free nitrate-based electrolyte was achieved within 5 min. This is a considerable technological advantage compared to several hours when using fluoride-based electrolytes

The optical properties of TNT layers were analyzed via UV–visible diffuse reflectance spectrometer (UV-DRS, Figs. 3b and S4a). Due to the presence of etched Ti foil in the sample prepared in $E_{100\%}W_{0\%}$ electrolyte, the data processing related to the measurement of E_g could not be conducted. Nevertheless, in all other TNT layers a peak reflectance at 406 nm was detected. Highest peak reflectance was obtained for TNT layers prepared in $E_{0\%}W_{100\%}$. It is due to the fact that the nanotubular morphologies such as tube length, tube diameter, grain size, and crystal phases affect their optical properties [54,55]. According to the Tauc's plot (calculated for the indirect transition from the UV-DRS spectra (Fig. 3b), the E_g for all TNT layers was approx. 3.08 eV. We obtained similar E_g values in our recent report on TNT layers prepared in Ag, Sr, K, and Na-nitrates based electrolytes [23]. Interestingly, this value is lower than the bandgap of some of the reported TNT layers obtained in fluoride-based electrolytes (E_g of approx. 3.2 eV) [56,57]. Reduction in the E_g on the TNT layers could be due to the potential decoration of metals/non-metals present in the nitrates-based electrolytes. The Ce was not detected by wavelength-dispersive X-ray spectroscopy (WDS) technique, hence we assume that concentration of Ce present in the TNT layers could be less than 0.01 wt%. Therefore, secondary-ion mass spectroscopy technique (SIMS) was used to detect the Ce in the TNT layers. An energy offset was used to suppress the Ti^{3+}ions that interfered with the Ce^{+} ions, to distinguish Ce^{+} ions from Ti^{3+} ions. Then Ce was clearly detected at 140 and 142 mass (a.m.u.), respectively (Fig. 3c), in the representative sample ($E_{75\%}W_{25\%}$). However, there was a deviation of the measured $^{140}Ce/^{142}Ce$ ratio from the natural abundance ratio in the mass spectrum in (Fig. 3c). Therefore, a test for the Ce^{+} secondary ion signal stability was performed (Fig. 3d) and revealed the decrease of the Ce^{+} intensities with the depth (sputtering time). Since in (Fig. 3d) the ^{142}Ce peak was measured about 170 s after the ^{140}Ce peak, a bias toward values of $^{140}Ce/^{142}Ce$ higher than the natural abundance ratio was created. Indeed, when the intensities of both isotopes were taken at the same time in (Fig. 3d), the ratio was close to 8 in agreement with the natural abundance ratio of ^{140}Ce and ^{142}Ce, which unambiguously proves the presence of Ce in the TNT layers. Interestingly, especially in the TNT layers the reduction in E_g could not only be attributed to elemental decoration but also through the structural changes. Indeed, combination of structural changes such as tube diameter [58–60], tube length [58–61], and porosity [62], affects the E_g of the TNT layers. For example, Murphy et al. observed the reduction in E_g with increasing in the tube length in the TNT layers [61]. Therefore, TNT layers with the longest tube length prepared in $E_{0\%}W_{100\%}$ had slightly lower E_g of ~3.04 eV when compared with the other TNT layers. Hence, we assume that the reduction in E_g in the TNT layers could be attributed to the structural features of the nanotubes and by the decoration of Ce.

At last, photocatalytic degradation of MB using the prepared TNT layers in $E_{100\%}W_{0\%}$, $E_{75\%}W_{25\%}$, $E_{50\%}W_{50\%}$, $E_{25\%}W_{75\%}$, and $E_{0\%}W_{100\%}$ electrolytes were investigated under UVA irradiation. The photocatalytic degradation using TNT layers follows the first-order reaction [63] and the degradation rates are summarized (Fig. 3e). The highest photocatalytic degradation rate is obtained for $E_{75\%}W_{25\%}$ ($k = 0.0151$ min^{-1}), followed by $E_{25\%}W_{75\%}$ ($k = 0.0133$ min^{-1}), $E_{50\%}W_{50\%}$ ($k = 0.0129$ min^{-1}), $E_{0\%}W_{100\%}$ ($k = 0.0105$ min^{-1}), and $E_{100\%}W_{0\%}$ ($k = 0.0062$ min^{-1}). These fluoride-free TNT layers showed a comparable photocatalytic performance in MB degradation with respect to fluoride-based TNT layers (Table S2). In general, for efficient photocatalytic degradation, a larger tube diameter is required for better pollutant diffusion within the tubes and an optimum tube length for increased light adsorption along the tube length [41]. Further, the mechanism of MB photodegradation was understood by studying the production of $HO^{\cdot}$ by fluorescence spectrophotometer using coumarin as a probe (Fig. 3f). Since, $HO^{\cdot}$ is considered the main reactive species in the photocatalytic process, e.g., for the degradation of organic pollutants and hydrogen production applications. HO are produced in the order of $E_{75\%}W_{25\%} > E_{0\%}W_{100\%} > E_{25\%}W_{75\%} > E_{50\%}W_{50\%} > E_{100\%}W_{0\%}$, similar to the photocatalytic degradation profiles. TNT layers grown in $E_{75\%}W_{25\%}$ electrolyte showed the highest photocatalytic degradation of MB, owing to their larger tube diameter, higher porosity, and higher surface roughness (Fig. 2), thereby increasing the number of catalytically active sites [48–51]. Moreover, with Ce decoration, there was a substantial increase in the photocatalytic degradation of MB when compared with the fluoride-free TNT layer grown in the $AgNO_3$ electrolyte, as reported in our previous work (Table S2). Evidently, TNT layers prepared in $E_{75\%}W_{25\%}$ showed the highest generation of HO. TNT layers prepared in $E_{100\%}W_{0\%}$ electrolyte showed the lowest production of $HO^{\cdot}$ due to the absence of nanotubular morphology (Fig. 1a) and the minor presence of TiO_2 (Fig. 3a) which resulted in the lowest MB degradation rate. Further, TNT layers prepared in $E_{50\%}W_{50\%}$ and $E_{25\%}W_{75\%}$ electrolytes showed similar photocatalytic degradation profiles. Indeed, both these TNT layers possess a similar number of catalytically active sites due to their similar porosity and surface roughness. Even though the TNT layer prepared in $E_{0\%}W_{100\%}$ possess similar porosity to $E_{50\%}W_{50\%}$ and $E_{25\%}W_{75\%}$, a higher photocatalytic activity was observed due to its longer nanotube length. Therefore, to obtain TNT with beneficial morphology for photocatalytic applications, it is crucially important to adjust the water content in fluoride-free nitrate-based electrolytes. Nevertheless, this report could pave the way for the use of eco-friendly nitrate-based electrolytes for the preparation of anodic TNT layers in the future with potential application in photocatalysis.

4. Conclusion

In summary, the presented work showed the eco-friendly preparation of TNT layers in an organic-aqueous-based electrolyte containing cerium ammonium nitrate via electrochemical anodization. The rapid growth of TNT layers up to 2.5 μm was observed within 5 min. The change of nanotubular morphology and surface features by varying the ratio of ethylene glycol and water in the electrolyte was studied for the first-time in fluoride-free nitrate-based electrolytes containing cerium. TNT layers prepared in $E_{75\%}W_{25\%}$ electrolyte possessed the optimal features for photocatalytic applications, i.e., large tube diameter, high porosity, and high surface roughness, thus leading to higher generation of $HO^{\cdot}$ and efficient degradation of MB. In a broader context, this study will help in preparing efficient TNT layers in fluoride-free nitrate-based electrolytes for photocatalytic applications.

CRediT authorship contribution statement

Guru Karthikeyan Thirunavukkarasu: Conceptualization, Investigation, Methodology, Visualization, Writing – review & editing. **Muhammad Bilal Hanif:** Investigation, Methodology, Visualization. **Viktoriia Liapun:** Investigation, Methodology, Visualization. **Karol Hensel:** Funding acquisition, Methodology, Writing – review & editing. **Jaroslav Kupčík:** Investigation, Methodology, Visualization. **Jan Lorincik:** Investigation, Methodology, Visualization. **Ivan Elantyev:** Investigation, Methodology, Visualization. **Olivier Monfort:** Funding acquisition, Methodology, Visualization, Writing – review & editing. **Martin Motola:** Funding acquisition, Supervision, Conceptualization, Visualization, Writing – review & editing.

Declaration of Competing Interest

The authors declare that they have no known competing financial interests or personal relationships that could have appeared to influence the work reported in this paper.

Data availability

Data will be made available on request.

Acknowledgement

This study was supported by the Operation Program of Integrated Infrastructure for the project, UpScale of Comenius University Capacities and Competence in Research, Development and Innovation, ITMS2014+: 313021BUZ3, co-financed by the European Regional Development Fund.This work was also supported by (i) Slovak Research and Development Agency (APVV) through the projects under contract No. APVV-21-0039 and APVV-20-0566, (ii) Scientific Grant Agency of the Slovak Ministry of Education, Sciences, Research and Sport (VEGA) through the projects No. 1/0319/23 and 1/0822/21, and (iii) We acknowledge CzechNanoLab Research Infrastructure supported by MEYS CR (LM2023051). This work was also supported by Programme to Support Prospective Human Resources – post Ph.D. candidates from the Czech Academy of Sciences under project no: L200322301. The SIMS and SEM-WDS results were obtained using the CICRR infrastructure, which is financially supported by the Ministry of Education, Youth and Sports of the Czech Republic - project LM2023041.

Supplementary materials

Supplementary material associated with this article can be found, in the online version, at doi:10.1016/j.materresbull.2023.112322.

References

[1] M. Assefpour-Dezfuly, C. Vlachos, E.H. Andrews, Oxide morphology and adhesive bonding on titanium surfaces, J. Mater. Sci. 19 (1984) 3626–3639, https://doi.org/10.1007/BF02396935.
[2] K. Lee, A. Mazare, P. Schmuki, One-dimensional titanium dioxide nanomaterials: nanotubes, Chem. Rev. 114 (2014) 9385–9454, https://doi.org/10.1021/cr500061m.
[3] K. Hashimoto, H. Irie, A. Fujishima, TiO_2 photocatalysis: a historical overview and future prospects, Jpn. J. Appl. Phys. 44 (2005) 8269–8285, https://doi.org/10.1143/JJAP.44.8269.
[4] S.Y. Lee, S.J. Park, TiO_2 photocatalyst for water treatment applications, J. Ind. Eng. Chem. 19 (2013) 1761–1769, https://doi.org/10.1016/j.jiec.2013.07.012.
[5] R. Daghrir, P. Drogui, D. Robert, Modified TiO_2 for environmental photocatalytic applications: a review, Ind. Eng. Chem. Res. 52 (2013) 3581–3599, https://doi.org/10.1021/ie303468t.
[6] M. Pawar, S. Topcu Sendoğdular, P. Gouma, A brief overview of TiO_2 photocatalyst for organic dye remediation: case study of reaction mechanisms involved in Ce-TiO_2 photocatalysts system, J. Nanomater. 2018 (2018) 1–13, https://doi.org/10.1155/2018/5953609.
[7] J. Schneider, M. Matsuoka, M. Takeuchi, J. Zhang, Y. Horiuchi, M. Anpo, D. W. Bahnemann, Understanding TiO_2 photocatalysis: mechanisms and materials, Chem. Rev. 114 (2014) 9919–9986, https://doi.org/10.1021/cr5001892.
[8] T. Rojviroon, O. Rojviroon, S. Sirivithayapakorn, S. Angthong, Application of TiO_2 nanotubes as photocatalysts for decolorization of synthetic dye wastewater, Water Resour. Ind. 26 (2021), 100163, https://doi.org/10.1016/j.wri.2021.100163.
[9] H. Yu, X. Wang, H. Sun, M. Huo, Photocatalytic degradation of malathion in aqueous solution using an Au–Pd–TiO_2 nanotube film, J. Hazard. Mater. 184 (2010) 753–758, https://doi.org/10.1016/j.jhazmat.2010.08.103.
[10] R. Liu, L. Sun, Y. Qiao, Y. Bie, P. Wang, X. Zhang, Q. Zhang, Efficient photocatalytic degradation of pharmaceutical pollutants using plasma-treated g-C_3N_4/TiO_2, Energy Technol. 8 (2020), 2000095, https://doi.org/10.1002/ente.202000095.
[11] M.P. Shah, Biological Treatment of Industrial Wastewater, ed., The Royal Society of Chemistry, 2021, https://doi.org/10.1039/9781839165399.
[12] N. Morin-Crini, E. Lichtfouse, G. Liu, V. Balaram, A.R.L. Ribeiro, Z. Lu, F. Stock, E. Carmona, M.R. Teixeira, L.A. Picos-Corrales, J.C. Moreno-Piraján, L. Giraldo, C. Li, A. Pandey, D. Hocquet, G. Torri, G. Crini, Worldwide cases of water pollution by emerging contaminants: a review, Environ. Chem. Lett. 20 (2022) 2311–2338, https://doi.org/10.1007/s10311-022-01447-4.
[13] P. Roy, S. Berger, P. Schmuki, TiO_2 nanotubes: synthesis and applications, Angew. Chem. Int. Ed. 50 (2011) 2904–2939, https://doi.org/10.1002/anie.201001374.
[14] J.M. Macák, H. Tsuchiya, P. Schmuki, High-aspect-ratio TiO_2 nanotubes by anodization of titanium, Angew. Chem. Int. Ed. 44 (2005) 2100–2102, https://doi.org/10.1002/anie.200462459.
[15] D. Wang, Y. Liu, B. Yu, F. Zhou, W. Liu, TiO_2 nanotubes with tunable morphology, diameter, and length: synthesis and photo-electrical/catalytic performance, Chem. Mater. 21 (2009) 1198–1206, https://doi.org/10.1021/cm802384y.
[16] R. Hahn, H. Lee, D. Kim, S. Narayanan, S. Berger, P. Schmuki, Self-organized anodic TiO_2-nanotubes in fluoride free electrolytes, ECS Trans. 16 (2008) 369–373, https://doi.org/10.1149/1.2982577.
[17] R. Hahn, J.M. Macak, P. Schmuki, Rapid anodic growth of TiO_2 and WO_3 nanotubes in fluoride free electrolytes, Electrochem. Commun. 9 (2007) 947–952, https://doi.org/10.1016/j.elecom.2006.11.037.
[18] D. Regonini, C.R. Bowen, A. Jaroenworaluck, R. Stevens, A review of growth mechanism, structure and crystallinity of anodized TiO_2 nanotubes, Mater. Sci. Eng. R Rep. 74 (2013) 377–406, https://doi.org/10.1016/j.mser.2013.10.001.
[19] K. Indira, U.K. Mudali, T. Nishimura, N. Rajendran, A review on TiO_2 nanotubes: influence of anodization parameters, formation mechanism, properties, corrosion behavior, and biomedical applications, J. Bio Tribo Corros. 1 (2015) 28, https://doi.org/10.1007/s40735-015-0024-x.
[20] I.B. Solangi, S. Memon, M.I. Bhanger, Removal of fluoride from aqueous environment by modified Amberlite resin, J. Hazard. Mater. 171 (2009) 815–819, https://doi.org/10.1016/j.jhazmat.2009.06.072.
[21] M. Flury, A. Papritz, Bromide in the natural environment: occurrence and toxicity, J. Environ. Qual. 22 (1993) 747–758, https://doi.org/10.2134/jeq1993.00472425002200040017x.
[22] J.R.F. Elphick, K.D. Bergh, H.C. Bailey, Chronic toxicity of chloride to freshwater species: effects of hardness and implications for water quality guidelines, Environ. Toxicol. Chem. 30 (2011) 239–246, https://doi.org/10.1002/etc.365.
[23] M.B. Hanif, G.K. Thirunavukkarasu, V. Liapun, H. Makarov, M. Gregor, T. Roch, T. Plecenik, K. Hensel, M. Sihor, O. Monfort, M. Motola, Fluoride-free synthesis of anodic TiO_2 nanotube layers: a promising environmentally friendly method for efficient photocatalysts, Nanoscale 14 (2022) 11703–11709, https://doi.org/10.1039/D2NR03379H.
[24] S. Cao, W. Huang, L. Wu, M. Tian, Y. Song, On the interfacial adhesion between TiO_2 nanotube array layer and Ti substrate, Langmuir 34 (2018) 13888–13896, https://doi.org/10.1021/acs.langmuir.8b03408.
[25] N. Lu, J. Zhang, Y. Dan, M. Sun, T. Gong, X. Li, X. Zhu, Growth of porous anodic TiO_2 in silver nitrate solution without fluoride: evidence against the field-assisted dissolution reactions of fluoride ions, Electrochem. Commun. 126 (2021), 107022, https://doi.org/10.1016/j.elecom.2021.107022.
[26] N. Ohtsu, M. Bai, K. Yamaguchi, Anomalous anodic layer growth on titanium occurring in electrolyte comprising nitrate and water, Surf. Coat. Technol. 374 (2019) 65–71, https://doi.org/10.1016/j.surfcoat.2019.05.032.
[27] R. Zhu, C. Li, P. Li, X. Shen, J. Chen, Y. Song, X. Zhu, Debunking the formation mechanism of nanopores in four kinds of electrolytes without fluoride ion, Electrochem. Commun. 129 (2021), 107093, https://doi.org/10.1016/j.elecom.2021.107093.
[28] J.M. Albella, I. Montero, J.M. Martinez-Duart, A theory of avalanche breakdown during anodic oxidation, Electrochim. Acta 32 (1987) 255–258, https://doi.org/10.1016/0013-4686(87)85032-6.
[29] X.F. Zhu, Y. Song, L. Liu, C.Y. Wang, J. Zheng, H.B. Jia, X.L. Wang, Electronic currents and the formation of nanopores in porous anodic alumina, Nanotechnology 20 (2009), 475303, https://doi.org/10.1088/0957-4484/20/47/475303.
[30] J.E. Houser, K.R. Hebert, The role of viscous flow of oxide in the growth of self-ordered porous anodic alumina films, Nat. Mater. 8 (2009) 415–420, https://doi.org/10.1038/nmat2423.
[31] S.J. Garcia-Vergara, P. Skeldon, G.E. Thompson, H. Habazaki, A flow model of porous anodic film growth on aluminium, Electrochim. Acta 52 (2006) 681–687, https://doi.org/10.1016/j.electacta.2006.05.054.
[32] G.K. Thirunavukkarasu, S. Gowrisankaran, M. Caplovicova, L. Satrapinskyy, M. Gregor, A. Lavrikova, J. Gregus, R. Halko, G. Plesch, M. Motola, O. Monfort, Contribution of photocatalytic and Fenton-based processes in nanotwin structured anodic TiO_2 nanotube layers modified by Ce and V, Dalton Trans. 51 (2022) 10763–10772, https://doi.org/10.1039/D2DT00829G.
[33] G.K. Thirunavukkarasu, O. Monfort, M. Motola, M. Motlochová, M. Gregor, T. Roch, M. Čaplovicová, A.Y. Lavrikova, K. Hensel, V. Brezová, M. Jerigová, J. Šubrt, G. Plesch, Ce ion surface-modified TiO_2 aerogel powders: a comprehensive study of their excellent photocatalytic efficiency in organic pollutant removal, New J. Chem. 45 (2021) 4174–4184, https://doi.org/10.1039/D0NJ05976E.
[34] S. Berger, J. Kunze, P. Schmuki, A.T. Valota, D.J. LeClere, P. Skeldon, G. E. Thompson, Influence of water content on the growth of anodic TiO_2 nanotubes in fluoride-containing ethylene glycol electrolytes, J. Electrochem. Soc. 157 (2010) C18, https://doi.org/10.1149/1.3251338.
[35] Y. Sun, Q. Zhao, G. Wang, K. Yan, Influence of water content on the formation of TiO_2 nanotubes and photoelectrochemical hydrogen generation, J. Alloy. Compd. 711 (2017) 514–520, https://doi.org/10.1016/j.jallcom.2017.03.007.
[36] A.G. Kontos, A.I. Kontos, D.S. Tsoukleris, V. Likodimos, J. Kunze, P. Schmuki, P. Falaras, Photo-induced effects on self-organized TiO_2 nanotube arrays: the influence of surface morphology, Nanotechnology 20 (2009), 045603, https://doi.org/10.1088/0957-4484/20/4/045603.
[37] C. Adán, J. Marugán, E. Sánchez, C. Pablos, R. van Grieken, Understanding the effect of morphology on the photocatalytic activity of TiO_2 nanotube array electrodes, Electrochim. Acta 191 (2016) 521–529, https://doi.org/10.1016/j.electacta.2016.01.088.
[38] H. Song, K. Cheng, H. Guo, F. Wang, J. Wang, N. Zhu, M. Bai, X. Wang, Effect of ethylene glycol concentration on the morphology and catalytic properties of TiO_2 nanotubes, Catal. Commun. 97 (2017) 23–26, https://doi.org/10.1016/j.catcom.2017.04.005.
[39] H. Liang, X. Li, Effects of structure of anodic TiO_2 nanotube arrays on photocatalytic activity for the degradation of 2,3-dichlorophenol in aqueous

solution, J. Hazard. Mater. 162 (2009) 1415–1422, https://doi.org/10.1016/j.jhazmat.2008.06.033.
[40] L. Qin, Q. Chen, R. Lan, R. Jiang, X. Quan, B. Xu, F. Zhang, Y. Jia, Effect of anodization parameters on morphology and photocatalysis properties of TiO_2 nanotube arrays, J. Mater. Sci. Technol. 31 (2015) 1059–1064, https://doi.org/10.1016/j.jmst.2015.07.012.
[41] C.B.D. Marien, T. Cottineau, D. Robert, P. Drogui, TiO_2 Nanotube arrays: influence of tube length on the photocatalytic degradation of Paraquat, Appl. Catal. B 194 (2016) 1–6, https://doi.org/10.1016/j.apcatb.2016.04.040.
[42] Q.A. Nguyen, Y.V. Bhargava, T.M. Devine, Titania nanotube formation in chloride and bromide containing electrolytes, Electrochem. Commun. 10 (2008) 471–475, https://doi.org/10.1016/j.elecom.2008.01.010.
[43] Q. Zhou, D. Niu, X. Feng, A. Wang, Z. Ying, J. Zhang, N. Lu, J. Zhu, X. Zhu, Debunking the effect of water content on anodizing current: evidence against the traditional dissolution theory, Electrochem. Commun. 119 (2020), 106815, https://doi.org/10.1016/j.elecom.2020.106815.
[44] L. Tsui, T. Homma, G. Zangari, Photocurrent conversion in anodized TiO_2 nanotube arrays: effect of the water content in anodizing solutions, J. Phys. Chem. C 117 (2013) 6979–6989, https://doi.org/10.1021/jp400318n.
[45] H. Sopha, M. Baudys, L. Hromadko, M. Lhotka, D. Pavlinak, J. Krysa, J.M. Macak, Scaling up anodic TiO_2 nanotube layers – Influence of the nanotube layer thickness on the photocatalytic degradation of hexane and benzene, Appl. Mater. Today 29 (2022), 101567, https://doi.org/10.1016/j.apmt.2022.101567.
[46] K. Zhu, N.R. Neale, A. Miedaner, A.J. Frank, Enhanced charge-collection efficiencies and light scattering in dye-sensitized solar cells using oriented TiO_2 nanotubes arrays, Nano Lett. 7 (2007) 69–74, https://doi.org/10.1021/nl062000o.
[47] P. Quitério, A. Apolinário, C.T. Sousa, J.D. Costa, J. Ventura, J.P. Araújo, The cyclic nature of porosity in anodic TiO_2 nanotube arrays, J. Mater. Chem. A 3 (2015) 3692–3698, https://doi.org/10.1039/C4TA04607B.
[48] Q.C. Xu, D.V. Wellia, S. Yan, D.W. Liao, T.M. Lim, T.T.Y. Tan, Enhanced photocatalytic activity of C–N-codoped TiO_2 films prepared via an organic-free approach, J. Hazard. Mater. 188 (2011) 172–180, https://doi.org/10.1016/j.jhazmat.2011.01.088.
[49] M. Coto, S.C. Troughton, P. Knight, R. Joshi, R. Francis, R.V. Kumar, T.W. Clyne, Optimization of the microstructure of TiO_2 photocatalytic surfaces created by Plasma Electrolytic Oxidation of titanium substrates, Surf. Coat. Technol. 411 (2021), 127000, https://doi.org/10.1016/j.surfcoat.2021.127000.
[50] C. Zhang, U. Chaudhary, S. Das, A. Godavarty, A. Agarwal, Effect of porosity on photocatalytic activity of plasma-sprayed TiO_2 coating, J. Therm. Spray Technol. 22 (2013) 1193–1200, https://doi.org/10.1007/s11666-013-9964-1.
[51] N. Arconada, Y. Castro, A. Durán, Photocatalytic properties in aqueous solution of porous TiO_2-anatase films prepared by sol–gel process, Appl. Catal. A 385 (2010) 101–107, https://doi.org/10.1016/j.apcata.2010.06.051.
[52] Y. Lin, Q. Qian, Z. Chen, D. Feng, P.D. Tuan, F. Yin, Surface modification of TiO_2 nanotubes prepared by porous titanium anodization via hydrothermal reaction: a method for synthesis high-efficiency adsorbents of recovering Sr ions, Langmuir 38 (2022) 11354–11361, https://doi.org/10.1021/acs.langmuir.2c01645.
[53] P. Acevedo-Peña, I. González, Relation between morphology and photoelectrochemical performance of TiO_2 nanotubes arrays grown in ethylene glycol/water, Procedia Chem. 12 (2014) 34–40, https://doi.org/10.1016/j.proche.2014.12.038.
[54] T. Hoseinzadeh, Z. Ghorannevis, M. Ghoranneviss, A.H. Sari, M.K. Salem, Effects of various applied voltages on physical properties of TiO_2 nanotubes by anodization method, J. Theor. Appl. Phys. 11 (2017) 243–248, https://doi.org/10.1007/s40094-017-0257-9.
[55] Z. Liu, Q. Zhang, L.C. Qin, Reduction in the electronic band gap of titanium oxide nanotubes, Solid State Commun. 141 (2007) 168–171, https://doi.org/10.1016/j.ssc.2006.09.055.
[56] M. Motola, M. Čaplovičová, M. Krbal, H. Sopha, G.K. Thirunavukkarasu, M. Gregor, G. Plesch, J.M. Macak, Ti^{3+} doped anodic single-wall TiO_2 nanotubes as highly efficient photocatalyst, Electrochim. Acta 331 (2020), 135374, https://doi.org/10.1016/j.electacta.2019.135374.
[57] M. Sihor, M.B. Hanif, G.K. Thirunavukkarasu, V. Liapun, M.F. Edelmannova, T. Roch, L. Satrapinskyy, T. Pleceník, S. Rauf, K. Hensel, O. Monfort, M. Motola, Anodization of large area Ti: a versatile material for caffeine photodegradation and hydrogen production, Catal. Sci. Technol. 12 (2022) 5045–5052, https://doi.org/10.1039/D2CY00593J.
[58] T. Tenkyong, J. Sahaya Selva Mary, B. Praveen, K. Pugazhendhi, D.J. Sharmila, J. M. Shyla, Structural modulation and band gap optimisation of electrochemically anodised TiO_2 nanotubes, Mater. Sci. Semicond. Process. 83 (2018) 150–158, https://doi.org/10.1016/j.mssp.2018.04.032.
[59] F.M. Hossain, A.V. Evteev, I.V. Belova, J. Nowotny, G.E. Murch, Electronic and optical properties of anatase TiO_2 nanotubes, Comput. Mater. Sci. 48 (2010) 854–858, https://doi.org/10.1016/j.commatsci.2010.04.007.
[60] M. Motola, L. Hromadko, J. Prikryl, H. Sopha, M. Krbal, J.M. Macak, Intrinsic properties of high-aspect ratio single- and double-wall anodic TiO_2 nanotube layers annealed at different temperatures, Electrochim. Acta 352 (2020), 136479, https://doi.org/10.1016/j.electacta.2020.136479.
[61] A. Murphy, Band-gap determination from diffuse reflectance measurements of semiconductor films, and application to photoelectrochemical water-splitting, Sol. Energy Mater. Sol. Cells 91 (2007) 1326–1337, https://doi.org/10.1016/j.solmat.2007.05.005.
[62] G.K. Mor, O.K. Varghese, M. Paulose, C.A. Grimes, Transparent highly ordered TiO_2 nanotube arrays via anodization of titanium thin films, Adv. Funct. Mater. 15 (2005) 1291–1296, https://doi.org/10.1002/adfm.200500096.
[63] J.M. Macak, M. Zlamal, J. Krysa, P. Schmuki, Self-organized TiO_2 nanotube layers as highly efficient photocatalysts, Small 3 (2007) 300–304, https://doi.org/10.1002/smll.200600426.